Disentanglement of Spin-Orbit Torques in Pt/Co Bilayers with the Presence of Spin Hall Effect and Rashba-Edelstein Effect

Ye Du,[1,2] Hiromu Gamou,[1] Saburo Takahashi,[3] Shutaro Karube,[1,4] Makoto Kohda,[1,2,4] and Junsaku Nitta[1,2,4,*]

[1] *Department of Materials Science, Tohoku University, Sendai 980-8579, Japan*

[2] *Organization for Advanced Studies, Center for Science and Innovation in Spintronics (Core Research Cluster), Tohoku University, Sendai 980-8577, Japan*

[3] *Advanced Institute for Materials Research, Tohoku University, Sendai 980-8577, Japan*

[4] *Center for Spintronics Research Network, Tohoku University, Sendai 980-8577, Japan*

(Received 31 July 2019; revised manuscript received 28 February 2020; accepted 23 March 2020; published 6 May 2020)

We demonstrate a quantitative disentanglement of current-induced spin-orbit torques (SOTs) in Pt/Co bilayers, where both the spin Hall effect (SHE) and the Rashba-Edelstein effect (REE) are present. The SOTs originating from the SHE in bulk Pt and from the REE at substrate (sub.)/Pt and Pt/Co interfaces are successfully disentangled and quantified utilizing harmonic Hall measurements, by taking advantage of different characteristic lengths between the two effects during spin-current transport. The fieldlike (FL) torque in our samples originates from the REE, while both SHE and REE contribute to the dampinglike (DL) torque. The experimentally extracted transport characteristic lengths in bulk Pt (an effective spin-diffusion length) are 1.8–3.0 nm, while those at Pt interfaces (an effective REE thickness) are 0.2–0.6 nm. The extracted REE-induced FL torque (and DL torque) efficiencies at sub./Pt and Pt/Co interfaces are of the same order of magnitude, but of opposite signs, which is consistent with the REE scenario. The origin of the observed temperature-dependent SOT sign reversal is clarified with our disentanglement analysis, demonstrating the significant role of the REE at both sub./Pt and Pt/Co interfaces, in contributing to the overall SOTs, as the thickness of the heavy-metal layer is thinner than its spin-diffusion length or comparable to a REE thickness.

DOI: 10.1103/PhysRevApplied.13.054014

I. INTRODUCTION

Recent advances in the spin Hall effect (SHE) [1–4] enable new functionalities in magnetic heterostructures with the presence of strong spin-orbit coupling. The pure spin currents generated by strong spin-orbit materials, such as heavy metals [5–9] and topological insulators [10,11], exert spin-orbit torques (SOTs) [12–15] on the neighboring ferromagnetic layer and act as the driving force for the control of local magnetic states, such as magnetization switching [6,8,9,16–18] and fast domain wall motion [19,20]. The SOT in heavy-metal/ferromagnet bilayers is understood based on the theory of Slonczewski-Berger spin-transfer torques [21,22] and can be decomposed into two orthogonal components, a (anti-)dampinglike (DL) term and a fieldlike (FL) term, having the forms of $\mathbf{m} \times (\boldsymbol{\sigma} \times \mathbf{m})$ and $\mathbf{m} \times \boldsymbol{\sigma}$, respectively, where $\mathbf{m}$ is the magnetization vector and $\boldsymbol{\sigma}$ is the spin polarization vector. Conventionally, the DL torque is considered to originate from the bulk SHE [8,23], following Slonczewski's theoretical model [24], while the FL torque is associated with the Rashba-Edelstein effect (REE) [25,26], an interfacial effect that is induced by the broken inversion symmetry [27]. However, a complete landscape on the origin of the SOT seems to be far more complicated: theoretical studies [28,29] have also shown that a nontrivial DL torque can be produced by the interfacial REE, which stems from a combination of the Rashba spin-orbit coupling and the *s-d* exchange interaction between the REE-induced spin accumulation and the local magnetic moments [28]; in addition, the SHE is also theoretically proposed to induce a small FL torque [30–32]. Therefore, the DL and FL torque are severely *entangled* in heavy-metal/ferromagnet bilayers, with the presence of both strong bulk spin-orbit coupling and interfacial Rashba spin splitting [33].

A quantitative SOT analysis in heavy-metal/ferromagnet bilayers is experimentally feasible via a heavy-metal-thickness-dependent SOT measurement [12,34–37]. Taking Pt [38,39], a 5*d* metal with strong spin-orbit coupling, as an example, the DL torque stemming from the SHE is described by the following hyperbolic function [7,34,35]

*nitta@material.tohoku.ac.jp

derived from drift-diffusion theory [40]:

$$B_{\mathrm{DL}}^{\mathrm{SHE}} \approx B_{\mathrm{DL\,sat}}^{\mathrm{SHE}}[1 - \mathrm{sech}(t_{\mathrm{Pt}}/\lambda_{\mathrm{Pt}})], \quad (1)$$

where $B_{\mathrm{DL}}^{\mathrm{SHE}}$ is the SHE-induced DL torque obtained at a certain Pt thickness (t_{Pt}) and $B_{\mathrm{DL\,sat}}^{\mathrm{SHE}}$ is its saturated value; λ_{Pt} is an effective spin diffusion length in Pt, with a typical thickness of several nanometers [35,41–54]; and sech is the hyperbolic secant. Based on the drift-diffusion approach, the FL torque originating from the REE demonstrates a similar t_{Pt} dependence [32]:

$$B_{\mathrm{FL}}^{\mathrm{REE}} \approx B_{\mathrm{FL\,sat}}^{\mathrm{REE}}[1 - \mathrm{sech}(t_{\mathrm{Pt}}/d_{\mathrm{REE}})], \quad (2)$$

where $B_{\mathrm{FL}}^{\mathrm{REE}}$ is the REE-induced FL torque at a certain t_{Pt} and $B_{\mathrm{FL\,sat}}^{\mathrm{REE}}$ is its saturated value; d_{REE} is an effective REE thickness in Pt, which is typically several angstroms, characterizing the thickness of an interface layer where the Rashba charge-spin conversion takes place [55,56]. The much shorter d_{REE}, relative to that of λ_{Pt}, is mainly due to the robust electron-screening effect [57] at the Pt/ferromagnet interface.

Previous experimental SOT studies [7,34–36,58] on Pt/ferromagnet bilayers mainly discussed the DL torque with the SHE. This is suitable when bulk SOT overwhelms the interface SOT. However, as the heavy-metal layer thickness shrinks down to the thin limit (e.g., shorter than λ_{Pt} or even comparable to d_{REE}), the REE-induced DL torque has to be considered in addition to the SHE. It means that, with the presence of strong Rashba splitting, both the top interface (e.g., Pt/ferromagnet) and bottom interface [e.g., substrate (sub.)/Pt] play an important role in contributing to the overall DL torque. Notably, this also holds for the FL torque. In fact, several previous works [34,36,59] have demonstrated a temperature-(T) dependent anomalous SOT sign reversal, which may result from such a complicated SOT entanglement. However, up to now, the origin of such a SOT sign reversal has remained elusive; moreover, a unified, consistent picture of the current-induced SOT efficiencies and corresponding characteristic lengths for both SHE and REE, in heavy-metal/ferromagnet bilayers, is lacking.

Here, we present a quantitative disentanglement of SOTs in prototypical Pt/Co bilayers with the presence of the SHE and REE via detailed t_{Pt}- and T-dependent harmonic Hall measurements [12,13,58,60]. The SOTs and characteristic transport lengths induced by the SHE in bulk Pt and by the REE at sub./Pt and Pt/Co interfaces are successfully disentangled and quantified. The obtained SOTs are consistent, both in sign and in magnitude, with theoretical studies [30,32] that take into account both effects, demonstrating the unique feature of the SOTs induced by Rashba spin splitting [61].

II. EXPERIMENTAL METHODS

Epitaxial thin films of Pt(t_{Pt})/Co(1.95) (thickness in nanometers) are sputter deposited onto Al_2O_3(0001) substrates at room temperature before a 2 nm amorphous AlO_x layer is capped on top for protection. The AlO_x layer is deposited directly from an Al_2O_3 sputtering target. The epitaxial growth of Pt and Co layers is suggested by x-ray diffraction and reflection of high-energy electron diffraction measurements, as shown in Fig. 1(a). The average roughnesses at sub./Pt and Pt/Co interfaces are estimated to be 0.2 and 0.1 nm, respectively, by x-ray reflectivity measurements [Fig. 1(b)], demonstrating favorable interfacial flatness. All films in this study are in-plane magnetized. The saturation magnetization (M_s) of Co is measured by using a vibrating sample magnetometer and determined to be 1.17×10^6 A/m. The M_s is found to be independent of T [inset of Fig. 4(b)], which is consistent with a previous study [34] on in-plane-magnetized Pt/Co bilayers. Hall bar devices with a rectangular shape of 25 μm in length and 10 μm in width are patterned by photolithography and Ar-ion milling for harmonic Hall measurements.

Following the method reported by Avci *et al.* [58] to separate the current-induced SOTs and the thermoelectric effects in in-plane-magnetized heavy-metal/ferromagnet bilayers, we perform the analysis for the angular dependence of second-harmonic signals to extract the overall DL and FL torques in our samples. As shown in Fig. 2(a), a sinusoidal voltage with a constant amplitude is applied to the Hall bar device, and a fixed-amplitude external magnetic field is applied in the thin-film plane. Both in-phase first-harmonic and out-of-phase second-harmonic Hall voltages [12,58] are recorded, while the direction of the external magnetic field rotates with an angle φ with respect to the x axis. According to Avci *et al.* [58], the φ dependence of the first- and second-harmonic Hall

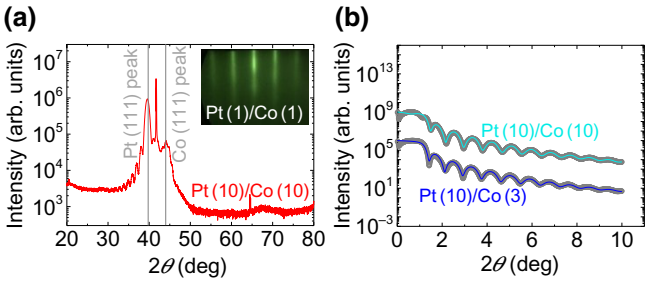

FIG. 1. (a) Out-of-plane x-ray diffraction pattern for thin films of Pt(10)/Co(10)/AlO_x(2) (thickness in nanometer) deposited onto Al_2O_3(0001) substrate. Inset shows the reflection of high-energy electron diffraction pattern for Pt(1)/Co(1) bilayers. (b) X-ray reflectivity patterns for Pt(10)/Co(3) and Pt(10)/Co(10). Average interfacial roughness is about 0.2 nm for the sub./Pt interface and 0.1 nm for the Pt/Co interface.

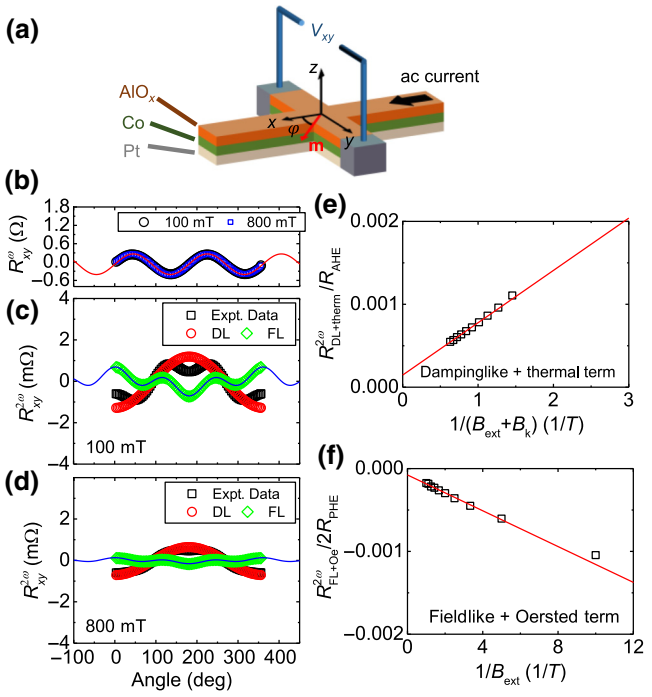

FIG. 2. (a) Schematic demonstration of the in-plane harmonic Hall measurement setup utilized in this study. (b) Angular dependence of the first-harmonic Hall resistance at 100 and 800 mT. Angular dependence of the second-harmonic Hall resistance and corresponding dampinglike (DL) and fieldlike (FL) components at 100 mT (c) and 800 mT (d). (e) DL plus thermoelectric terms of second-harmonic Hall resistance, normalized by anomalous Hall resistance, plotted against the inverse static field (external magnetic field, B_{ext}, plus out-of-plane anisotropy field, B_k). (f) FL plus Oersted field terms of the second-harmonic Hall resistance, normalized by planar Hall resistance, plotted against inverse B_{ext}.

resistance (R^{ω} and $R^{2\omega}$, respectively) is

$$R^{\omega}_{xy} = R_{PHE} \sin 2\varphi, \tag{3}$$

$$R^{2\omega}_{xy} = -\left(R_{AHE}\frac{B_{DL}}{B_{ext}+B_k} + R^{TE}_{\nabla T}\right)\cos\varphi + 2R_{PHE}(2\cos^3\varphi - \cos\varphi)\frac{B_{FL}+B_{Oe}}{B_{ext}}, \tag{4}$$

where R_{PHE} and R_{AHE} are the planar Hall resistance and anomalous Hall resistance; B_{DL} and B_{FL} are the overall DL and FL effective magnetic fields (denoted as DL and FL torque hereafter for consistency); B_{ext}, B_k, and B_{Oe} are the external magnetic field, out-of-plane anisotropy field, and heavy-metal-layer-induced Oersted field; and $R^{TE}_{\nabla T}$ is the second-harmonic resistance induced by thermal effects, such as the anomalous Nernst effect and the spin Seebeck effect [62]. As an example, the SOT analysis of the Hall bar device, with a stacking structure of Pt(2.25)/Co(1.95)/AlO_x(2) is shown in Figs. 2(b)–2(f): the DL plus thermal term of the second-harmonic signal is obtained by fitting the experimental data at $\varphi = 45°$, 135°, 225°, and 315° with the $\cos\varphi$ function [see circles in Figs. 2(c) and 2(d)]; the DL term is subsequently obtained by performing the B_{ext}-dependent measurement shown in Fig. 2(e), where DL torque is accessible via the slope of the linear fitting. The FL plus Oersted field term is obtained by subtracting the DL term from the φ-dependent second-harmonic data [see rhombuses, Figs. 2(c) and 2(d)], where the FL torque is obtained via the field-dependent linear fitting [Fig. 2(f)] after subtracting the Oersted field contribution [63]. The measured DL and FL torque data for Pt/Co bilayers are summarized in Figs. 3(c) and 3(e).

III. SPIN-ORBIT TORQUE DISENTANGLEMENT

Figure 3(a) demonstrates the schematic model for the SOT disentanglement in this study. The bulk Pt region and sub./Pt and Pt/Co interfaces are considered as sources of SOTs because of strong spin-orbit coupling in Pt and the concomitant large Rashba spin splitting. Each spin-current source produces a DL torque and a FL torque, that is, B_{DL0} and B_{FL0} for bulk Pt, B_{DL1} and B_{FL1} for the sub./Pt interface, and B_{DL2} and B_{FL2} for the Pt/Co interface. The effective REE thickness at the sub./Pt and Pt/Co interfaces is denoted as d_{REE1} and d_{REE2}, respectively. Prior to SOT analysis, the Hall bar resistance of each device is examined. Figures 3(b) and 3(d) show the normalized inverse sheet resistance ($1/R^0_{xx}$) and the corresponding Pt resistivity (ρ_{Pt}) as a function of t_{Pt} and T. The $1/R^0_{xx}$ value is measurable at a very thin t_{Pt} of 0.23 nm, suggesting very flat interfaces that are consistent with the x-ray reflectivity results. The ρ_{Pt} value shows a sudden drop near $t_{Pt} = 1.1$ and 4.0 nm, for which we propose two possible origins. One possible origin is that interfacial electron scattering decreases with increasing t_{Pt}, contributing to a decrease in ρ_{Pt}; the other is that, as t_{Pt} increases, there is an abrupt decrease in the local dislocation density [64] at a certain t_{Pt} (e.g., around 1.1 and 4.0 nm) for each of the sub./Pt and Pt/Co interfaces caused by an incoherent interfacial strain relaxation in epitaxial samples. We argue that the latter origin is more likely to dominate. This is because we do not observe such an abrupt $1/R^0_{xx}$ change in polycrystalline Pt/Co bilayers (see the Supplemental Material [63]), where interfacial electron scattering persists, while interfacial strain is coherently relaxed via grain boundaries. It is also worth noting that we do not find any significant phase change in Pt with varying t_{Pt} up to 10 nm [63]; in addition, a similar sudden resistivity drop was previously observed in epitaxial Ta-based heterostructure thin films [64].

The t_{Pt}- and T-dependent current-induced SOTs, normalized by current density estimated in Pt (J_{Pt}), are summarized in Figs. 3(c) and 3(e). Qualitatively, the DL torque (B_{DL}) and FL torque (B_{FL}) exhibit a significant difference

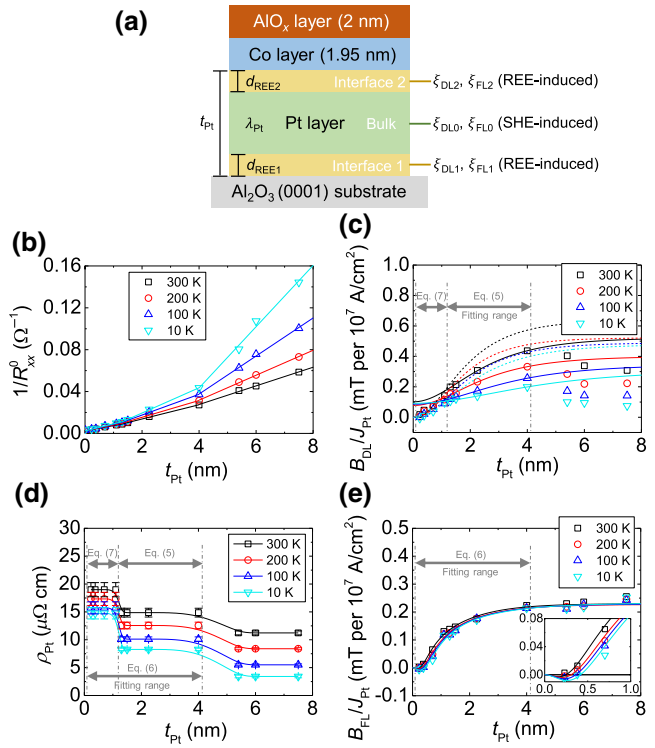

FIG. 3. (a) Schematic illustration of the SOT entanglement in Pt/Co bilayers. Current-induced DL and FL torque efficiencies arise from Pt bulk region (ξ_{DL0} and ξ_{FL0}), substrate/Pt interface (ξ_{DL1} and ξ_{FL1}), and Pt/Co interface (ξ_{DL2} and ξ_{FL2}). Pt thickness t_{Pt} dependence of normalized inverse sheet resistance $1/R^0_{xx}$ (b) and resistivity ρ_{Pt} (d) at 10–300 K. Solid lines in (b) are linear fits to data for $t_{Pt} = 0.2$–1.1, 1.3–4.0, and 4.0–7.5 nm, respectively; solid lines in (d) are a guide to the eye. (c),(e) t_{Pt} dependence of DL torque B_{DL} (c) and FL torque B_{FL} (e) normalized by Pt current density at 10–300 K. Solid lines in (c) are fits to data for $t_{Pt} = 1.3$–4.0 nm via Eq. (5); dashed lines in (c) are fits to data for $t_{Pt} = 0.2$–1.1 nm via Eq. (7); solid lines in (e) are fits to data with $t_{Pt} = 0.2$–4.0 nm via Eq. (6), where thin t_{Pt} data and fitting lines are shown in the inset.

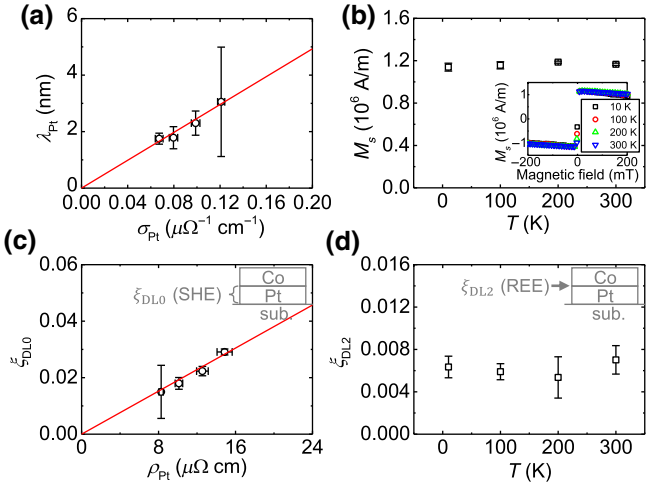

FIG. 4. (a) Pt spin-diffusion length λ_{Pt} as a function of Pt conductivity σ_{Pt}. (b) Temperature dependence of saturation magnetization (M_s) for Pt(3)/Co(3) bilayers. Inset to (b) shows typical M-H curves at 10–300 K. (c) DL torque efficiency ξ_{DL0} in bulk Pt as a function of Pt resistivity ρ_{Pt}. Solid lines in (a) and (c) are linear fits to data. (d) Temperature dependence of REE-induced DL torque efficiency ξ_{DL2} at the Pt/Co interface.

in T: the DL torque decreases dramatically with decreasing T for $t_{Pt} > 1.3$ nm, while the FL torque barely changes over all thickness and T ranges, suggesting that they have very different origins. Notably, the signs of both DL and FL torque agree with previous SOT studies [58,65] on in-plane-magnetized Pt/ferromagnet bilayers. A quantitative disentanglement of the SOTs in Pt/Co bilayers, as mentioned above, requires one to take into account the bulk SHE in Pt and the REE at sub./Pt and Pt/Co interfaces. Because the experimentally obtained SOT in single-layer Co is found to be negligibly small [63], we consider that the SOT induced by the Co/AlO$_x$ interface in this work is trivial. By considering that both SHE and REE contribute to the DL torque [28,29], the following equation is used to fit the DL torque in Fig. 3(c) in the intermediate t_{Pt} region (the least-squares method is used for all fittings throughout this work):

$$\begin{aligned} B_{DL} &\approx B_{DL\,Pt\,bulk} + B_{DL\,Pt/Co} \\ &\approx B_{DL0}[1 - \mathrm{sech}(t_{Pt}/\lambda_{Pt})] + B_{DL2} \\ &\quad (\text{fitting range: } 1.3\text{–}4.0\,\text{nm}), \end{aligned} \tag{5}$$

where B_{DL0} is the saturated SHE-induced DL torque and B_{DL2} is the saturated DL torque generated at the Pt/Co interface due to the REE. The DL and FL torque efficiencies, ξ_{DL} and ξ_{FL}, are calculated via $\xi_{DL(FL)} = (2eM_st_F)/\hbar B_{DL(FL)\,sat}/J_{Pt}$, in which e is the electron charge, t_F is the Co layer thickness, and $\hbar$ is the reduced Planck constant. Notably, the effective REE thickness at the Pt/Co interface is estimated to be much smaller than that of such a t_{Pt} range (e.g., ~0.4 nm is assumed for a Bi/Ag Rashba interface [55]), and therefore, the hyperbolic term for B_{DL2} in Eq. (5) is neglected. In addition, the DL torque originating from the sub./Pt interface is estimated to be much smaller than the two terms in Eq. (5) in this t_{Pt} range and neglected because of the spin relaxation in Pt. The fitting results [Figs. 4(a) and 4(c)] demonstrate the Elliot-Yafet spin-relaxation mechanism [35,66–68] and an intrinsic (or perhaps side-jump) contribution to the SHE [4,68] in the Pt layer. The intrinsic (or side-jump) SHE mechanism is consistent with the results shown in Fig. 3(c) that, for a particular T, the decrease in the DL torque for $t_{Pt} > 4.0$ nm is accompanied by a drop in ρ_{Pt} [Fig. 3(d)]. Notably, the spin-relaxation mechanism here reflects mainly the bulk

property, and is different from a previous weak antilocalization study [69], in which Pt layer is fabricated very differently (e.g., high deposition T) and measured at a lower T. A small and positive ξ_{DL2} is found at the Pt/Co interface [Fig. 4(d)], which is consistent in sign with theoretical calculations [32].

The DL torque is dominated by the SHE with $t_{Pt} > 1.3$ nm, as suggested by a gradual saturation of DL torque with increasing t_{Pt} and a rapid drop with decreasing T. The T-independent FL torque in the same t_{Pt} region, on the other hand, shows strong evidence that the FL torque is independent of the spin currents generated by the SHE. Particularly, at $t_{Pt} = 7.5$ nm, the FL torque remains almost constant, while the DL torque decreases by a factor of three when T drops from 300 to 10 K [see Figs. 3(c) and 3(e)]. Therefore, the FL torque originates overwhelmingly from the REE and not the SHE. One may argue that the SHE generates a T-independent FL torque. That, however, is contrary to theoretical calculations [31,32] that the SHE-induced FL torque, if any, should scale with the magnitude of the SHE-induced spin currents. By assuming this scaling relationship, the SHE-induced FL torque efficiency (ξ_{FL0}) is estimated to be smaller than 0.0004. Comparing this value with ξ_{DL0} in Fig. 4(c), one finds a qualitative consistency with theoretical calculations [30,32] that ξ_{FL0}/ξ_{DL0} is roughly determined by $\mathrm{Im}[G_{mix}]/\mathrm{Re}[G_{mix}]$ [32], in which G_{mix} is the spin-mixing conductance. Based on the discussions above, the FL torque in our samples stems predominantly from the REE at sub./Pt and Pt/Co interfaces. Thus, the t_{Pt} dependence of B_{FL} is quantitatively analyzed using the following fitting equation based on the drift-diffusion approach (see the Supplemental Material [63] for a discussion on the biresistivity issue in Pt) [32,70]:

$$\begin{aligned} B_{FL} &\approx B_{FL\,sub/Pt} + B_{FL\,Pt/Co} \\ &\approx B_{FL1}[1 - \mathrm{sech}(t_{Pt}/d_{REE1})]\mathrm{sech}(t_{Pt}/\lambda'_{Pt}) \\ &\quad + B_{FL2}[1 - \mathrm{sech}(t_{Pt}/d_{REE2})] \\ &\quad (\text{fitting range: } 0.2\text{–}4.0\,\text{nm}), \end{aligned} \tag{6}$$

where B_{FL1} and B_{FL2} are the REE-induced saturated FL torque originating from sub./Pt and Pt/Co interfaces, respectively; λ'_{Pt}, the spin diffusion length for $t_{Pt} = 0.2$–1.1 nm, is obtained based on the λ_{Pt}-conductivity (σ_{Pt}) linear relationship in Fig. 4(a). As a result, the extracted d_{REE1} and d_{REE2} [Fig. 5(b)] values are reasonable for a Rashba interface [55,56]; the corresponding ξ_{FL1} and ξ_{FL2} [Fig. 5(a)] values at sub./Pt and Pt/Co interfaces are found to be independent of the SHE-induced spin currents (ξ_{DL0}), which confirms again that the FL torque in our samples originates from the REE, not the SHE. Moreover, ξ_{FL1} and ξ_{FL2} are of the same order of magnitude, but of opposite signs. Such a sign reversal is consistent with the REE scenario [25,26]: the REE-induced $\boldsymbol{\sigma}$ is proportional to the cross product of the electron momentum vector $\mathbf{k}$ and the interfacial electric field vector $\mathbf{E}$, where $\mathbf{E}$ is induced by the broken inversion symmetry [27] and has its direction along the film normal. The REE-induced FL torque, having the form of $\mathbf{m} \times \boldsymbol{\sigma}$, is an odd function of $\boldsymbol{\sigma}$. Therefore, a reversal of polarity in $\mathbf{E}$ ultimately leads to a sign change in ξ_{FL}. Because of the large work function in Pt, $\mathbf{E}$ is expected to have a direction pointing from Pt to Co for the Pt/Co interface and from Pt to $Al_2O_3(0001)$ sub. for the sub./Pt interface due to orbital hybridization [71].

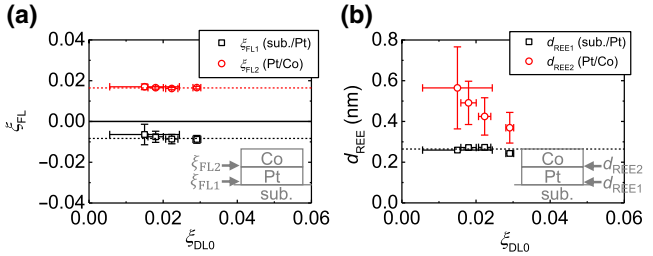

FIG. 5. (a) FL torque efficiencies ξ_{FL1} and ξ_{FL2} and (b) effective REE thicknesses d_{REE1} and d_{REE2} at sub./Pt, Pt/Co interfaces plotted as a function of DL torque efficiency in bulk Pt (ξ_{DL0}). ξ_{FL} and d_{REE} are extracted from the nonlinear fitting in Fig. 3(e) via Eq. (6). Dashed lines in (a) and (b) are a guide to the eye.

With both d_{REE1} and d_{REE2} obtained in Fig. 5(b), the REE-induced ξ_{DL} [28,29] from the sub./Pt (ξ_{DL1}) interface is examined by fitting the DL torque for a thin t_{Pt} region [dashed lines in Fig. 3(c)]:

$$\begin{aligned} B_{DL} &\approx B_{DL\,sub/Pt} + B_{DL\,Pt\,bulk} + B_{DL\,Pt/Co} \\ &\approx B_{DL1}[1 - \mathrm{sech}(t_{Pt}/d_{REE1})]\mathrm{sech}(t_{Pt}/\lambda'_{Pt}) \\ &\quad + B_{DL2}[1 - \mathrm{sech}(t_{Pt}/d_{REE2})] \\ &\quad + B'_{DL0}[1 - \mathrm{sech}(t_{Pt}/\lambda'_{Pt})] \\ &\quad (\text{fitting range: } 0.2\text{–}1.1\,\text{nm}), \end{aligned} \tag{7}$$

where B_{DL1}, the only fitting parameter, is the saturated DL torque from sub./Pt via the REE. B'_{DL0} is the saturated SHE-induced DL torque for $t_{Pt} = 0.2$–1.1 nm and is estimated based on the ξ_{DL0}-ρ_{Pt} linear relationship in Fig. 4(c). As a result, the experimentally extracted ξ_{DL1} and ξ_{DL2} [Fig. 6(a)] are of opposite sign and are consistent with the respective sign of ξ_{FL1} and ξ_{FL2}, reflecting a sign change in $\mathbf{E}$ when comparing sub./Pt and Pt/Co interfaces. The extracted SOT efficiencies and corresponding characteristic lengths are summarized in Table. I.

IV. DISCUSSION

A. Spin Transport Characteristic Lengths

The combined effects of the bulk SHE in Pt and the interfacial REE at sub./Pt and Pt/Co interfaces vigorously explain the t_{Pt}- and T-dependent DL and FL torques shown in Figs. 3(c) and 3(e). The overall DL or FL torques measured at a specific t_{Pt} are

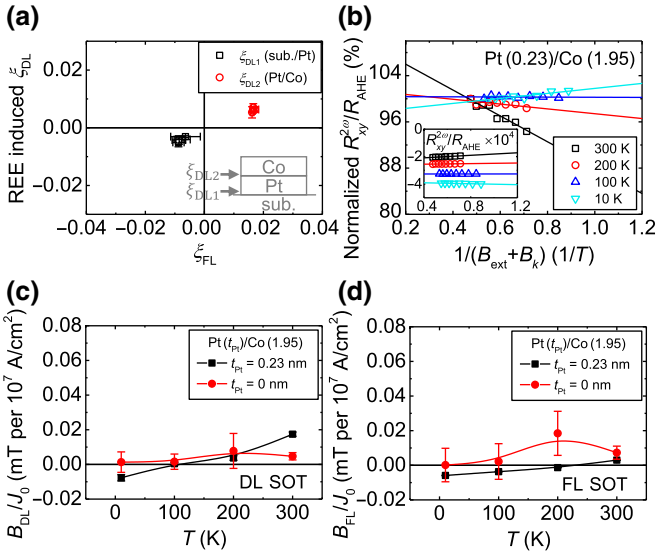

FIG. 6. (a) REE-induced DL torque efficiencies ξ_{DL1} and ξ_{DL2} at sub./Pt and Pt/Co interfaces plotted as a function of corresponding FL torque efficiencies ξ_{FL1} and ξ_{FL2}. Opposite signs of SOT efficiencies at sub./Pt and Pt/Co interfaces suggest a reversal of the interfacial electric field vector. (b) Normalized DL plus thermoelectric terms of second-harmonic signal as a function of the inverse of static field (external field B_{ext} plus out-of-plane anisotropy field B_k). Solid lines are linear fits to data. Inset shows raw data and linear fits at each temperature. (c),(d) Temperature dependence of overall DL (c) and FL (d) SOTs with $t_{Pt} = 0.23$ nm and $t_{Pt} = 0$ nm normalized by current density J_0, where J_0 is an estimated current density in Pt for Pt-inserted sample and in Co for Pt-free sample. Solid lines are a guide to the eye.

quantitatively explained by competition from the three SOT sources mentioned above (although the bulk-induced FL torque is negligible), depending not only on the saturated charge-spin conversion efficiencies in the bulk or at interfaces, but also on the corresponding characteristic lengths (i.e., d_{REE1}, d_{REE2}, and λ_{Pt}). The nonlinear fitting in Fig. 3(e) via Eq. (6) provides a reliable determination of the characteristic transport lengths of the REE [d_{REE1} and d_{REE2}, Fig. 5(b)] because the Pt layer should be flat and homogeneous for most of the data points due to the interfacial smoothness of our Pt/Co thin films. As a result, d_{REE1} is found to be smaller than that of either d_{REE2} or λ_{Pt} [Figs. 4(a) and 5(b)], meaning that the charge-spin conversion at the sub./Pt interface via the REE, compared with the other two SOT sources, is accomplished within the smallest length scale. This indicates that the charge-spin conversion at the sub./Pt interface (the negative SOT source) may dominate the overall SOT when t_{Pt} becomes comparable to d_{REE1}, which is consistent with the T-dependent SOT sign reversal observed at 10 K in this study with $t_{Pt} = 0.23$ nm [Figs. 6(b)–6(d)]. We emphasize that we do not intend to discuss the sign reversal using SOT data of a specific $t_{Pt} = 0.23$ nm, where the Pt layer is likely to be inhomogeneous because 0.23 nm is comparable to half of the fcc Pt unit cell; instead, we argue that the T-dependent SOT sign reversal observed in this study is mainly determined by the negative SOT source at the sub./Pt interface [Fig. 6(a)], with a very small d_{REE1}, which is obtained via nonlinear fitting over a relatively wide t_{Pt} range. Our results are highly consistent with previous studies [34,36,59], where the SOT sign reversal occurs only at low T or with a very thin heavy-metal layer thickness, when the SOT originating from the bulk SHE is significantly suppressed.

In particular, we note here that, while this work demonstrates an experimental extraction of d_{REE} [Fig. 5(b)] via a SOT characterization, the extracted d_{REE} (e.g., $d_{REE1} =$ 0.2–0.3 nm) value is somewhat larger than a theoretically calculated Thomas-Fermi screening length for an

TABLE I. Summary of the characteristic lengths and saturated dampinglike and fieldlike SOT efficiencies for Pt bulk and sub./Pt and Pt/Co interfaces obtained from the disentanglement analysis in this work. The characteristic length represents an effective spin-diffusion length for bulk Pt and an effective REE thickness for sub./Pt and Pt/Co interfaces.

SOT source	Temperature (K)	Pt resistivity ($\mu\Omega$ cm)	Characteristic length (nm)	Dampinglike SOT efficiency	Fieldlike SOT efficiency
Pt bulk	300	14.87	1.75	0.029	(abs.) < 0.0004
Pt bulk	200	12.56	1.78	0.022	(abs.) < 0.0004
Pt bulk	100	10.12	2.30	0.018	(abs.) < 0.0004
Pt bulk	10	8.27	3.05	0.015	(abs.) < 0.0004
sub./Pt interface	300		0.23	−0.005	−0.009
sub./Pt interface	200		0.26	−0.004	−0.009
sub./Pt interface	100		0.26	−0.004	−0.008
sub./Pt interface	10		0.26	−0.003	−0.006
Pt/Co interface	300		0.34	0.007	0.017
Pt/Co interface	200		0.40	0.005	0.016
Pt/Co interface	100		0.44	0.006	0.017
Pt/Co interface	10		0.51	0.006	0.017

idealized metallic surface [72], which is typically less than 0.1 nm. Despite such a discrepancy, we argue the validity of the obtained d_{REE} with following two points: (1) Inevitably, our sputter-deposited films suffer from an imperfection of interfaces because of interfacial roughness ($R_{rms} = 0.1$–0.2 nm) and possible interlayer atomic mixing at sub./Pt and Pt/Co interfaces. Such an interfacial imperfection, in return, is very likely to cause a broadening of the Rashba interfacial scattering potential, where, in theoretical calculations [30–32], such a potential is often localized at the interface by using a Dirac delta function. Consequently, the broadening of the scattering potential results in a broadened interface region for electron screening and subsequently an enhancement in d_{REE}. An earlier study [55] on spin-charge conversion at the Bi/Ag interface assumed a similar d_{REE} of 0.4 nm, which supports this argument. (2) Theoretical calculations by Zhang [57] show that the screening length can be enhanced, when the asymmetry in the spin-dependent density of states is lifted by interfacial magnetic moments. This qualitatively supports our results because the extracted d_{REE2} (Pt/Co interface, with magnetism) is larger than that of d_{REE1} (sub./Pt interface, without magnetism), as shown in Fig. 5(b). Based on the discussions above, we believe that our experimentally extracted d_{REE}, although larger than a typical Thomas-Fermi screening length for an ideal interface, is a reasonable spin-transport length for the REE charge-spin conversion in our sputter-deposited Pt/Co bilayers.

V. Spin-Orbit Torque Efficiencies

The result that the SHE-induced DL torque efficiency ξ_{DL0} in our Pt/Co/AlO_x thin film scales with ρ_{Pt} (intrinsic or perhaps side-jump SHE mechanisms) shown in Fig. 4(c) agrees well with a previous SOT study [73] on in-plane-magnetized Pt/Co_2FeAl/MgO samples. However, this ρ_{Pt} scaling is distinctly different from what is observed in perpendicularly magnetized Pt/Co/MgO [34] or Pt/Hf/(Co, Fe)B/MgO [36] thin films possessing a thinner ferromagnetic layer, in which the ξ_{DL0} is ρ_{Pt} independent. Such a discrepancy between the in-plane-magnetized and perpendicularly magnetized samples can be explained by the effect of spin backflow at the ferromagnet/oxide interface: a recent ferromagnetic resonance study by Ghosh *et al.* [74] has demonstrated a characteristic length of about 1.2 nm in a ferromagnetic layer for an efficient absorption of transverse spin current. Due to relatively thick Co layer of 1.95 nm in our samples, the SHE-induced transverse spin current is expected to be completely absorbed in the Co layer via spin-momentum transfer, and the spin backflow at the ferromagnet/oxide interface is minimal. However, in the case of perpendicularly magnetized samples, where the ferromagnetic layer thickness is typically less than 1.2 nm [34,36], spin backflow occurs at the ferromagnet/oxide interface because of an incomplete spin absorption, thereby partially cancelling out the spin current across the Pt/ferromagnet interface [75]. Due to such a parasitic effect, the measured T-dependent SOT efficiencies in perpendicularly magnetized samples may not reflect the intrinsic charge-spin conversion in a heavy metal or at the heavy-metal/ferromagnet interface.

The experimentally obtained T-independent FL torque in this study is consistent with the fact that the FL torque in our samples originates from the REE. This is because thermal excitations at room temperature are expected to be much smaller than the energy of the (interfacial) spin-orbit coupling; therefore, one does not expect a dramatic change in the Rashba spin accumulation at sub./Pt or Pt/Co interfaces that ultimately affects the FL torque as T changes. The T-independent FL torque is consistent with a previous SOT study on Pt/Co/MgO [34] thin films.

Also, we discuss the influence of the magnetic proximity effect (MPE) on both DL and FL torque. As for the DL torque, we show in Fig. 7(a) that ξ_{DL0} in our samples has the same ρ_{Pt} scaling relationship as that of previous Pt-based SOT studies [7,34,35,44,46,50,51,54,58,65,68] and,

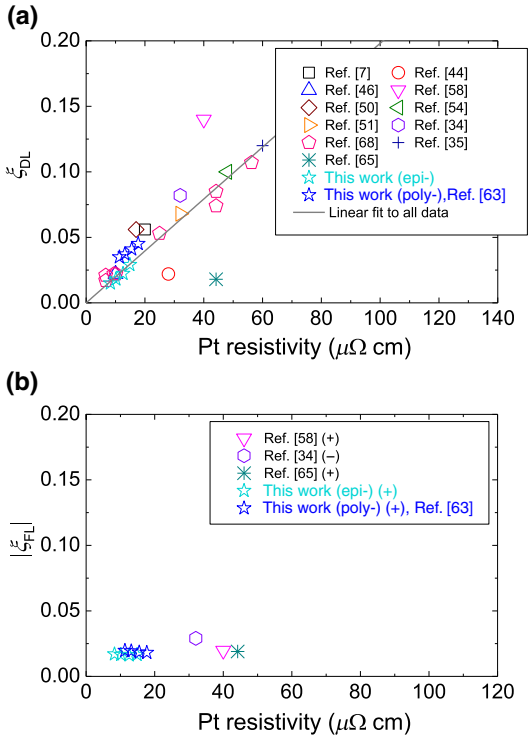

FIG. 7. Summary of (a) DL torque efficiencies and (b) FL torque efficiencies as a function of Pt resistivity for previous Pt-based SOT studies and for this work. Data of this work shown in (a) are the spin Hall effect induced DL torque efficiency (ξ_{DL0}); data of this work shown in (b) are the Rashba-Edelstein effect induced FL torque efficiency (ξ_{FL2}); "+" and "−" in (b) denote signs of each FL torque efficiency.

particularly, a previous study by Sagasta *et al.* [68], using Pt-based lateral spin valves, where Pt and ferromagnet layers are separated by using a nonlocal geometry and MPE is absent. This strongly suggests that the MPE on the DL torque in our Pt/Co bilayers is negligible. For the FL torque, as no significant T dependence is shown [Fig. 3(e)] and the magnitude agrees with previous studies as shown in Fig. 7(b) [34,58,65], we consider that the effect of MPE on FL torque is small as well. Such an irrelevance of MPE to the SOT is consistent with a recent study by Zhu *et al.* [76].

VI. OUTLOOK

The REE is shown in this study to play a critical role in contributing to the overall SOT, as heavy-metal thickness is comparable to d_{REE}. An accurate determination of d_{REE} may be possible via magnetotransport studies for atomically flat oxide interfaces [77,78], where interfacial scattering potential is more localized by using sharper interfaces compared with our films deposited at room temperature. Due to the nontrivial contribution of REE to the current-induced SOT, it would also be intriguing to investigate the gate control [77,79–81] of spin-orbitronic devices with ultrathin layer thickness, which is a favorable feature for high-density information storage scaling.

VII. CONCLUSIONS

We present a quantitative disentanglement of the current-induced SOTs originating from the SHE and REE in Pt/Co bilayers. The SOTs originating from the SHE in bulk Pt and from the REE at sub./Pt and Pt/Co interfaces are successfully disentangled and quantified. The REE-induced ξ_{FL1} and ξ_{FL2} (and also ξ_{DL1} and ξ_{DL2}) at sub./Pt and Pt/Co interfaces are of the same order of magnitude, but opposite signs, which is consistent with the REE model. The experimentally extracted characteristic spin-transport lengths in Pt bulk (i.e., an effective spin-diffusion length, λ_{Pt}) are in the order of nanometers, while those at sub./Pt and Pt/Co interfaces (i.e., an effective REE thickness, d_{REE1} and d_{REE2}) are in the order of angstroms. The SOT sign reversal at low T as t_{Pt} approaches the thin limit is explained by the dominant negative SOTs induced by the REE at the sub./Pt interface. Our results provide a unified picture of SOTs in prototypical Pt/Co bilayers, with the presence of both the SHE and REE, illustrating the significant role of the REE in contributing to current-induced SOTs, as the heavy-metal layer thickness is thinner than its spin-diffusion length or comparable to a REE thickness.

ACKNOWLEDGMENTS

We are grateful to Byong-Guk Park, Jeongchun Ryu, Vivek Amin, Mark Stiles, and Yong-Chang Lau for helpful discussions. This work is supported by the Japanese Ministry of Education, Culture, Sports, Science, and Technology (MEXT) in Grant-in-Aid for Scientific Research (Grant No. 15H05699) and the JSPS Core-to-Core program.

[1] M. I. Dyakonov and V. I. Perel, Current-induced spin orientation of electrons in semiconductors, Phys. Lett. A **35**, 459 (1971).
[2] J. E. Hirsch, Spin Hall Effect, Phys. Rev. Lett. **83**, 1834 (1999).
[3] S. Zhang, Spin Hall Effect in the Presence of Spin Diffusion, Phys. Rev. Lett. **85**, 393 (2000).
[4] J. Sinova, S. O. Valenzuela, J. Wunderlich, C. H. Back, T. Jungwirth, and Spin Hall effects. Rev. Mod. Phys. **87**, 1213 (2015).
[5] T. Tanaka, H. Kontani, M. Naito, T. Naito, D. S. Hirashima, K. Yamada, and J. Inoue, Intrinsic spin Hall effect and orbital Hall effect in 4d and 5d transition metals, Phys. Rev. B **77**, 165117 (2008).
[6] I. M. Miron, K. Garello, G. Gaudin, P.-J. Zermatten, M. V. Costache, S. Auffret, S. Bandiera, B. Rodmacq, A. Schuhl, and P. Gambardella, Perpendicular switching of a single ferromagnetic layer induced by in-plane current injection, Nature **476**, 189 (2011).
[7] L. Liu, T. Moriyama, D. C. Ralph, and R. A. Buhrman, Spin-Torque Ferromagnetic Resonance Induced by the Spin Hall Effect, Phys. Rev. Lett. **106**, 036601 (2011).
[8] L. Liu, C.-F. Pai, Y. Li, H. W. Tseng, D. C. Ralph, and R. A. Buhrman, Spin-Torque switching with the giant spin Hall effect of tantalum, Science **336**, 555 (2012).
[9] C.-F. Pai, L. Liu, Y. Li, H. W. Tseng, D. C. Ralph, and R. A. Buhrman, Spin transfer torque devices utilizing the giant spin Hall effect of tungsten, Appl. Phys. Lett. **101**, 122404 (2012).
[10] M. Z. Hasan and C. L. Kane, Colloquium: Topological insulators, Rev. Mod. Phys. **82**, 3045 (2010).
[11] X.-L. Qi and S.-C. Zhang, Topological insulators and superconductors, Rev. Mod. Phys. **83**, 1057 (2011).
[12] J. Kim, J. Sinha, M. Hayashi, M. Yamanouchi, S. Fukami, T. Suzuki, S. Mitani, and H. Ohno, Layer thickness dependence of the current-induced effective field vector in Ta|CoFeB|MgO, Nat. Mater. **12**, 240 (2013).
[13] K. Garello, I. M. Miron, C. O. Avci, F. Freimuth, Y. Mokrousov, S. Blügel, S. Auffret, O. Boulle, G. Gaudin, and P. Gambardella, Symmetry and magnitude of spin–orbit torques in ferromagnetic heterostructures, Nat. Nanotechnol. **8**, 587 (2013).
[14] X. Fan, J. Wu, Y. Chen, M. J. Jerry, H. Zhang, and J. Q. Xiao, Observation of the nonlocal spin-orbital effective field, Nat. Commun. **4**, 1799 (2013).
[15] A. Manchon, J. Železný, I. M. Miron, T. Jungwirth, J. Sinova, A. Thiaville, K. Garello, and P. Gambardella, Current-induced spin-orbit torques in ferromagnetic and antiferromagnetic systems, Rev. Mod. Phys. **91**, 035004 (2019).
[16] Y. Fan, P. Upadhyaya, X. Kou, M. Lang, S. Takei, Z. Wang, J. Tang, L. He, L.-T. Chang, M. Montazeri, G. Yu, W. Jiang, T. Nie, R. N. Schwartz, Y. Tserkovnyak, and K. L. Wang, Magnetization switching through giant spin–orbit torque in

a magnetically doped topological insulator heterostructure, Nat. Mater. **13**, 699 (2014).

[17] A. R. Mellnik, J. S. Lee, A. Richardella, J. L. Grab, P. J. Mintun, M. H. Fischer, A. Vaezi, A. Manchon, E.-A. Kim, N. Samarth, and D. C. Ralph, Spin-transfer torque generated by a topological insulator, Nature **511**, 449 (2014).

[18] Y.-C. Lau, D. Betto, K. Rode, J. M. D. Coey, and P. Stamenov, Spin–orbit torque switching without an external field using interlayer exchange coupling, Nat. Nanotechnol. **11**, 758 (2016).

[19] K.-S. Ryu, L. Thomas, S.-H. Yang, and S. Parkin, Chiral spin torque at magnetic domain walls, Nat. Nanotechnol. **8**, 527 (2013).

[20] S. Emori, U. Bauer, S.-M. Ahn, E. Martinez, and G. S. D. Beach, Current-driven dynamics of chiral ferromagnetic domain walls, Nat. Mater. **12**, 611 (2013).

[21] J. C. Slonczewski, Current-driven excitation of magnetic multilayers, J. Magn. Magn. Mater. **159**, L1 (1996).

[22] L. Berger, Emission of spin waves by a magnetic multilayer traversed by a current, Phys. Rev. B **54**, 9353 (1996).

[23] X. Fan, H. Celik, J. Wu, C. Ni, K.-J. Lee, V. O. Lorenz, and J. Q. Xiao, Quantifying interface and bulk contributions to spin–orbit torque in magnetic bilayers, Nat. Commun. **5**, 3042 (2014).

[24] J. C. Slonczewski, Currents and torques in metallic magnetic multilayers, J. Magn. Magn. Mater. **247**, 324 (2002).

[25] Y. A. Bychkov and E. I. Rashba, Properties of a 2D electron gas with lifted spectral degeneracy, JETP Lett. **39**, 78 (1984).

[26] V. M. Edelstein, Spin polarization of conduction electrons induced by electric current in two-dimensional asymmetric electron systems, Solid State Commun. **73**, 233 (1990).

[27] I. M. Miron, G. Gaudin, S. Auffret, B. Rodmacq, A. Schuhl, S. Pizzini, J. Vogel, and P. Gambardella, Current-driven spin torque induced by the Rashba effect in a ferromagnetic metal layer, Nat. Mater. **9**, 230 (2010).

[28] X. Wang and A. Manchon, Diffusive Spin Dynamics in Ferromagnetic Thin Films with a Rashba Interaction, Phys. Rev. Lett. **108**, 117201 (2012).

[29] D. A. Pesin and A. H. MacDonald, Quantum kinetic theory of current-induced torques in Rashba ferromagnets, Phys. Rev. B **86**, 014416 (2012).

[30] P. M. Haney, H.-W. Lee, K.-J. Lee, A. Manchon, and M. D. Stiles, Current induced torques and interfacial spin-orbit coupling: Semiclassical modeling, Phys. Rev. B **87**, 174411 (2013).

[31] V. P. Amin and M. D. Stiles, Spin transport at interfaces with spin-orbit coupling: Formalism, Phys. Rev. B **94**, 104419 (2016).

[32] V. P. Amin and M. D. Stiles, Spin transport at interfaces with spin-orbit coupling: Phenomenology, Phys. Rev. B **94**, 104420 (2016).

[33] C. R. Ast, J. Henk, A. Ernst, L. Moreschini, M. C. Falub, D. Pacilé, P. Bruno, K. Kern, and M. Grioni, Giant Spin Splitting Through Surface Alloying, Phys. Rev. Lett. **98**, 186807 (2007).

[34] C.-F. Pai, Y. Ou, L. H. Vilela-Leão, D. C. Ralph, and R. A. Buhrman, Dependence of the efficiency of spin Hall torque on the transparency of Pt/ferromagnetic layer interfaces, Phys. Rev. B **92**, 064426 (2015).

[35] M.-H. Nguyen, D. C. Ralph, and R. A. Buhrman, Spin torque Study of the Spin Hall Conductivity and Spin Diffusion Length in Platinum Thin Films with Varying Resistivity, Phys. Rev. Lett. **116**, 126601 (2016).

[36] Y. Ou, C.-F. Pai, S. Shi, D. C. Ralph, and R. A. Buhrman, Origin of fieldlike spin-orbit torques in heavy metal/ferromagnet/oxide thin film heterostructures, Phys. Rev. B **94**, 140414 (2016).

[37] J. W. Lee, Y.-W. Oh, S.-Y. Park, A. I. Figueroa, G. van der Laan, G. Go, K.-J. Lee, and B.-G. Park, Enhanced spin-orbit torque by engineering Pt resistivity in Pt/Co/AlO_x structures, Phys. Rev. B **96**, 064405 (2017).

[38] E. Saitoh, M. Ueda, H. Miyajima, and G. Tatara, Conversion of spin current into charge current at room temperature: Inverse spin-Hall effect, Appl. Phys. Lett. **88**, 182509 (2006).

[39] T. Kimura, Y. Otani, T. Sato, S. Takahashi, and S. Maekawa, Room-Temperature Reversible Spin Hall Effect, Phys. Rev. Lett. **98**, 156601 (2007).

[40] P. C. van Son, H. van Kempen, and P. Wyder, Boundary Resistance of the Ferromagnetic-Nonferromagnetic Metal Interface, Phys. Rev. Lett. **58**, 2271 (1987).

[41] H. Kurt, R. Loloee, K. Eid, W. P. Pratt, and J. Bass, Spin-memory loss at 4.2 K in sputtered Pd and Pt and at Pd/Cu and Pt/Cu interfaces, Appl. Phys. Lett. **81**, 4787 (2002).

[42] M. Morota, Y. Niimi, K. Ohnishi, D. H. Wei, T. Tanaka, H. Kontani, T. Kimura, and Y. Otani, Indication of intrinsic spin Hall effect in 4d and 5d transition metals, Phys. Rev. B **83**, 174405 (2011).

[43] H. Nakayama, K. Ando, K. Harii, T. Yoshino, R. Takahashi, Y. Kajiwara, K. Uchida, Y. Fujikawa, and E. Saitoh, Geometry dependence on inverse spin Hall effect induced by spin pumping in $Ni_{81}Fe_{19}$/Pt films, Phys. Rev. B **85**, 144408 (2012).

[44] K. Kondou, H. Sukegawa, S. Mitani, K. Tsukagoshi, and S. Kasai, Evaluation of spin Hall angle and spin diffusion length by using spin current-induced ferromagnetic resonance, Appl. Phys. Express **5**, 073002 (2012).

[45] Z. Feng, J. Hu, L. Sun, B. You, D. Wu, J. Du, W. Zhang, A. Hu, Y. Yang, D. M. Tang, B. S. Zhang, and H. F. Ding, Spin Hall angle quantification from spin pumping and microwave photoresistance, Phys. Rev. B **85**, 214423 (2012).

[46] Y. Niimi, D. Wei, H. Idzuchi, T. Wakamura, T. Kato, and Y. Otani, Experimental Verification of Comparability Between Spin-Orbit and Spin-Diffusion Lengths, Phys. Rev. Lett. **110**, 016805 (2013).

[47] C. T. Boone, H. T. Nembach, J. M. Shaw, and T. J. Silva, Spin transport parameters in metallic multilayers determined by ferromagnetic resonance measurements of spin-pumping, J. Appl. Phys. **113**, 153906 (2013).

[48] H. Jiao and G. E. W. Bauer, Spin Backflow and AC Voltage Generation by Spin Pumping and the Inverse Spin Hall Effect, Phys. Rev. Lett. **110**, 217602 (2013).

[49] W. Zhang, V. Vlaminck, J. E. Pearson, R. Divan, S. D. Bader, and A. Hoffmann, Determination of the Pt spin diffusion length by spin-pumping and spin Hall effect, Appl. Phys. Lett. **103**, 242414 (2013).

[50] J. C. Rojas-Sánchez, N. Reyren, P. Laczkowski, W. Savero, J.-P. Attané, C. Deranlot, M. Jamet, J.-M. George, L.

Vila, and H. Jaffrès, Spin Pumping and Inverse Spin Hall Effect in Platinum: The Essential Role of Spin-Memory Loss at Metallic Interfaces, Phys. Rev. Lett. **112**, 106602 (2014).

[51] Y. Wang, P. Deorani, X. Qiu, J. H. Kwon, and H. Yang, Determination of Intrinsic Spin Hall Angle in Pt, Appl. Phys. Lett. **105**, 152412 (2014).

[52] H. Y. T. Nguyen, W. P. Pratt, and J. Bass, Spin-flipping in Pt and at Co/Pt interfaces, J. Magn. Magn. Mater. **361**, 30 (2014).

[53] Y. Liu, Z. Yuan, R. J. H. Wesselink, A. A. Starikov, and P. J. Kelly, Interface Enhancement of Gilbert Damping from First Principles, Phys. Rev. Lett. **113**, 207202 (2014).

[54] H. L. Wang, C. H. Du, Y. Pu, R. Adur, P. C. Hammel, and F. Y. Yang, Scaling of Spin Hall Angle in 3d, 4d, and 5d Metals from $Y_3Fe_5O_{12}$/Metal Spin Pumping, Phys. Rev. Lett. **112**, 197201 (2014).

[55] J. C. Rojas-Sánchez, L. Vila, G. Desfonds, S. Gambarelli, J. P. Attané, J. M. De Teresa, C. Magén, and A. Fert, Spin-to-charge conversion using Rashba coupling at the interface between non-magnetic materials, Nat. Commun. **4**, 2944 (2013).

[56] J. C. Rojas-Sánchez, S. Oyarzún, Y. Fu, A. Marty, C. Vergnaud, S. Gambarelli, L. Vila, M. Jamet, Y. Ohtsubo, A. Taleb-Ibrahimi, P. Le Fèvre, F. Bertran, N. Reyren, J.-M. George, and A. Fert, Spin to Charge Conversion at Room Temperature by Spin Pumping into a New Type of Topological Insulator: α -Sn Films, Phys. Rev. Lett. **116**, 096602 (2016).

[57] S. Zhang, Spin-Dependent Surface Screening in Ferromagnets and Magnetic Tunnel Junctions, Phys. Rev. Lett. **83**, 640 (1999).

[58] C. O. Avci, K. Garello, M. Gabureac, A. Ghosh, A. Fuhrer, S. F. Alvarado, and P. Gambardella, Interplay of spin-orbit torque and thermoelectric effects in ferromagnet/normal-metal bilayers, Phys. Rev. B **90**, 224427 (2014).

[59] J. Kim, J. Sinha, S. Mitani, M. Hayashi, S. Takahashi, S. Maekawa, M. Yamanouchi, and H. Ohno, Anomalous temperature dependence of current-induced torques in CoFeB/MgO heterostructures with Ta-based underlayers, Phys. Rev. B **89**, 174424 (2014).

[60] U. H. Pi, K. Won Kim, J. Y. Bae, S. C. Lee, Y. J. Cho, K. S. Kim, and S. Seo, Tilting of the spin orientation induced by Rashba effect in ferromagnetic metal layer, Appl. Phys. Lett. **97**, 162507 (2010).

[61] A. Manchon, H. C. Koo, J. Nitta, S. M. Frolov, and R. A. Duine, New perspectives for Rashba spin–orbit coupling, Nat. Mater. **14**, 871 (2015).

[62] K. Uchida, S. Takahashi, K. Harii, J. Ieda, W. Koshibae, K. Ando, S. Maekawa, and E. Saitoh, Observation of the spin Seebeck effect, Nature **455**, 778 (2008).

[63] See the Supplemental Material http://link.aps.org/supplemental/10.1103/PhysRevApplied.13.054014 for details on the current shunting and Oersted field correction, nonlinear fitting process, spin-orbit torques in other control samples, and transmission electron microscopy characterizations.

[64] H. Gamou, Y. Du, M. Kohda, and J. Nitta, Enhancement of spin current generation in epitaxial α-Ta/CoFeB bilayer, Phys. Rev. B **99**, 184408 (2019).

[65] Y.-C. Lau and M. Hayashi, Spin torque efficiency of Ta, W, and Pt in metallic bilayers evaluated by harmonic Hall and spin Hall magnetoresistance measurements, Jpn. J. Appl. Phys. **56**, 0802B5 (2017).

[66] R. J. Elliott, Theory of the effect of spin-orbit coupling on magnetic resonance in some semiconductors, Phys. Rev. **96**, 266 (1954).

[67] Y. Yafet, G factors and spin-lattice relaxation of conduction electrons, Solid State Phys. **14**, 1 (1963).

[68] E. Sagasta, Y. Omori, M. Isasa, M. Gradhand, L. E. Hueso, Y. Niimi, Y. Otani, and F. Casanova, Tuning the spin Hall effect of Pt from the moderately dirty to the superclean regime, Phys. Rev. B **94**, 060412(R) (2016).

[69] J. Ryu, M. Kohda, and J. Nitta, Observation of the D'yakonov-Perel' Spin Relaxation in Single-Crystalline Pt Thin Films, Phys. Rev. Lett. **116**, 256802 (2016).

[70] By setting $d_{\mathrm{REE1}}, d_{\mathrm{REE2}} > 0$ as the boundary conditions (this is natural as an interfacial layer thickness has to be large than 0) during the nonlinear fitting process for Eq. (6), one obtains the only solution for those four fitting parameters and their corresponding error bars as shown in Figs. 5(a) and 5(b) with the least squares fitting method.

[71] X. Chen, Y. Liu, G. Yang, H. Shi, C. Hu, M. Li, and H. Zeng, Giant antidamping orbital torque originating from the orbital Rashba-Edelstein effect in ferromagnetic heterostructures, Nat. Commun. **9**, 2569 (2018).

[72] D. M. Newns, Dielectric response of a semi-infinite degenerate electron gas, Phys. Rev. B **1**, 3304 (1970).

[73] T. A. Peterson, A. P. McFadden, C. J. Palmstrøm, and P. A. Crowell, Influence of the magnetic proximity effect on spin-orbit torque efficiencies in ferromagnet/platinum bilayers, Phys. Rev. B **97**, 020403 (2018).

[74] A. Ghosh, S. Auffret, U. Ebels, and W. E. Bailey, Penetration Depth of Transverse Spin Current in Ultrathin Ferromagnets, Phys. Rev. Lett. **109**, 127202 (2012).

[75] X. Qiu, W. Legrand, P. He, Y. Wu, J. Yu, R. Ramaswamy, A. Manchon, and H. Yang, Enhanced Spin-Orbit Torque via Modulation of Spin Current Absorption, Phys. Rev. Lett. **117**, 217206 (2016).

[76] L. J. Zhu, D. C. Ralph, and R. A. Buhrman, Irrelevance of magnetic proximity effect to spin-orbit torques in heavy-metal/ferromagnet bilayers, Phys. Rev. B **98**, 134406 (2018).

[77] E. Lesne, Y. Fu, S. Oyarzun, J. C. Rojas-Sánchez, D. C. Vaz, H. Naganuma, G. Sicoli, J.-P. Attané, M. Jamet, E. Jacquet, J.-M. George, A. Barthélémy, H. Jaffrès, A. Fert, M. Bibes, and L. Vila, Highly efficient and tunable spin-to-charge conversion through Rashba coupling at oxide interfaces, Nat. Mater. **15**, 1261 (2016).

[78] L. Liu, Q. Qin, W. Lin, C. Li, Q. Xie, S. He, X. Shu, C. Zhou, Z. Lim, J. Yu, W. Lu, M. Li, X. Yan, S. J. Pennycook, and J. Chen, Current-induced magnetization switching in all-oxide heterostructures, Nat. Nanotechnol. **14**, 939 (2019).

[79] J. Nitta, T. Akazaki, H. Takayanagi, and T. Enoki, Gate Control of Spin-Orbit Interaction in an Inverted $In_{0.53}Ga_{0.47}As/In_{0.52}Al_{0.48}As$ Heterostructure, Phys. Rev. Lett. **78**, 1335 (1997).

[80] S. Dushenko, M. Hokazono, K. Nakamura, Y. Ando, T. Shinjo, and M. Shiraishi, Tunable inverse spin Hall effect in nanometer-thick platinum films by ionic gating, Nat. Commun. **9**, 3118 (2018).

[81] R. Mishra, F. Mahfouzi, D. Kumar, K. Cai, M. Chen, X. Qiu, N. Kioussis, and H. Yang, Electric-field control of spin accumulation direction for spin-orbit torques, Nat. Commun. **10**, 248 (2019).